SIMULATION MODEL OF A MICROFLUIDIC POINT OF CARE BIOSENSOR FOR ELECTRICAL ENUMERATION OF BLOOD CELLS

BY

AARON JANKELOW

THESIS

Submitted in partial fulfillment of the requirements
for the degree of Master of Science in Bioengineering
in the Graduate College of the
University of Illinois at Urbana-Champaign, 2018

Urbana, Illinois

Adviser:

Professor Rashid Bashir

Abstract

Point of care microfluidic devices provide many opportunities for improving the diagnosis of a number of illnesses. They can provide a speedy, quantitative assay in the form of an easy to use portable platform. By using Finite Element Analysis software to model and simulate these microfluidic devices, we can further optimize and improve on the design of such devices. In this work we will use such software in order to model an electrical counting chamber that would be implemented in such a device. This chamber utilizes the coulter counting principle to measure the change in impedance caused when a bead or a cell passes over a series of electrodes. By utilizing the signals to count the number of cells coming into and out of a capture chamber that targets a specific antigen, we can obtain a quantitative measure of how many cells or beads were expressing the target antigen and use this for a diagnosis. First the simulation was tuned to be able to produce the characteristic bipolar pulse when a cell passed over the electrodes. Then by varying elements such as bead size, input voltage, bead composition and electrode placement and recording the results we can use this model to help further refine and optimize this device by giving us a quantitative model that will allow us to better understand how changing such variables will alter the signal received from the device and thus allow us a better understanding of the best way to get a clearer signal.

Table of Contents

1. Introduction

Sepsis is a potentially deadly complication of an infection that occurs when the body's immune response triggers an inflammation which causes a chain reaction that can lead to organ failure. About 20% of the over 5 million patients sent to the intensive care unit in the United States each year are diagnosed with severe sepsis [1]. The mortality rate of Sepsis is estimated to be between 28% and 50% [2]. A large part of the reason why sepsis is so deadly is the lack of a quick diagnostic tool that can be delivered at point of care (PoC) [3]. The current standard for diagnosis of sepsis involves culturing the pathogen for several days, leading to the disease progression outpacing the diagnostic process [4]. Each hour that passes without receiving a proper treatment decreases the chance of surviving the next 72 hours by about 7.6%, making treating sepsis as early as possible critical [5].

One solution to this problem is using point of care microfluidic devices to obtain the diagnosis quickly at a low expense. Microfluidic devices are rapidly advancing the field of clinical diagnostics through their ability to quickly and quantitatively assess biomarkers from very small physiological samples. Additionally, microfluidics allows for inexpensive tests that make it very attractive for use in developing parts of the world [6] [7]. A point of care device for the diagnosis of sepsis is currently being worked on that utilizes electrical counting and antibody-based capture in order to quantify the cell surface expression level of the CD64 antigen that is associated with sepsis [8]. In order for such a chip to function properly, it is vital that the cell counts are as accurate as possible, meaning a clear identifiable signal is vital.

The aim of this work is to use the Finite Element Analysis software COMSOL Multiphysics in order to simulate the electrical counting mechanism of a microfluidic device for the diagnosis of sepsis from whole blood. By changing aspects such as the particle size, particle composition, applied voltage and other relevant variables in this model, we will be able to figure out the optimal conditions for creating a high signal-to-noise ration signal which will help aid in the development of such a device. Additionally, because this model does not discriminate based on

the specific antigen, it should be possible to apply it to devices for the diagnosis of other illnesses.

1.1 Point of Care Devices

Point of care (PoC) devices are portable, in vitro diagnostic tests that can be used outside a laboratory setting to provide results [9]. These tests use microfluidic technology in order to analyze a number of possible analytical targets including proteins, nucleic acids, blood cells, pathogens, and more. These devices aim to be able to use a sample with little to no pre-preparation and do not require complicated instructions or training to use. A famous example of a PoC device are the glucose monitoring devices used in diabetes management that can quickly measure the blood glucose level taken from a drop of blood.

Work has also been done on developing PoC devices that measure the concentration of proteins in whole blood. This is important because blood is the tissue with the largest representation of the human proteome, and changes of the protein profile in plasma can be associated with a large number of human diseases [10]. PoC devices are expected to make a big impact on full blood counts, which are a common indicator of patient health [11]. A full blood count includes a white blood cell differential count, hemoglobin concentration, red blood cell count, and a platelet count. Work has been done to create a microfluidic PoC device that can provide a $CD4^+$ and $CD8^+$ T cell count from whole blood for the management of HIV/AIDS [12]. Testing has also been done on developing PoC microfluidic devices for the detection of myocardial infarctions from whole blood [13].

1.2 Flow Cytometry

Flow cytometry is the current standard for enumerating specific white blood cells and quantifying protein concentration on their surfaces [14]. This technique works by labeling the proteins of interest on the cell's surface with a fluorescent reporter, or fluorophore, that will emit light in a specific, narrow frequency. The tagged cells are illuminated by lasers to excite

the fluorophores and then the resulting fluorescence is measured by detectors (Fig. 1) [15]. As a cell with more of the target protein on its surface will have more attached fluorophores, the intensity of the fluorescence can be used to quantify the protein concentration on the cell surface.

This method does have its drawbacks however, which make it poorly suited for use in a PoC device. The device requires trained technicians, who may not always be available, to operate and is prohibitively expensive at over $50,000. Additionally, it is bulky and cannot easily be moved. These factors mean that we must look to other methods for use in an inexpensive point-of-care device.

1.3 Microfluidic Coulter Counters

Coulter Counters as a method of counting particles were first reported in the 1950s [16]. A coulter counter is an electrical counting device that can be used to count and differentiate particles based on size by flowing them through a small orifice that has an electrical current flowing through it. As the particle flows through the channel, it will cause a change in impedance proportional to the volume of the particle [17]. This change can be seen as a sharp spike on an electric current vs time plot (Fig 2) [18]. This occurs because of the difference between the conductivity of the particle and the surrounding liquid causes an increased resistance.

Coulter Counters are useful in PoC devices as they are easily miniaturized. Furthermore, researchers have been able to demonstrate that they can be created inexpensively by building them directly onto a cheap printed circuit board [19]. Researches have already shown the ability of coulter counters to perform cell sizing and differentiation of white blood cells in whole blood. Holmes et al demonstrated the ability to count white blood cells and separate them into monocytes, lymphocytes and neutrophils using a microfluidic coulter counter [20]. Watkins et al were able to make use of these properties of the coulter counter in a microfluidic device to count cells individually to provide accurate $CD4^+$ and $CD8^+$ cell counts [12]. These counts can be read by taking advantage of the bipolar pulse produced as each individual cell passes through the coulter counter (Fig. 3)

1.4 Computer Simulations

Simulation methodologies are a powerful tool for reducing the experimental workload and expense of research by allowing researchers to create and test a digital model of the product that is being designed. By creating an accurate computer model and then changing key variables, we gain the ability to optimize the system without performing a multitude of costly experiments. This allows us to reduce the amount of prototyping and even the ability to predict the success of a potential chip design before starting a single experiment [21].

Simulation software has been used to simulate a wide variety of phenomena involved in the development of lab-on-a-chip technology. Wolff et al used computer simulations to optimize a structure for hydrodynamic focusing in a microfluidic device [22]. Another study used software to simulate electroosmotic flow over nonuniform surfaces [23]. Chen et al used CFD-ACE+ software to simulate the flow dynamics for their *Drosophila* cell sorter [24].

Previous work has been done on simulating coulter counters for microfluidic devices. One study used COMSOL Multiphysics to simulate a microfluidic device where three cell types were introduced via three separate inlets, were mixed passively as they flowed through a mixing region, and then counted via a coulter counter [25]. The coulter counter was created by using a pair of parallel vertical electrodes along each side of a vertical ramp down channel. This study used COMSOL software to simulate the mixing of the different cell types in the mixing region as well as the electric field gradient in the channel from electric field generated by the two electrodes. Studies have also been done that utilized COMSOL to simulate the electric field, flow profile, and impedance signal through other microfluidic coulter counter designs [26]. Guo et al used COMSOL to measure the hydrodynamic and electrokinetic forces acting upon a particle moving through a micro-coulter counter [27]. Of note is that all of the previously mentioned designs for microfluidic coulter counters utilized parallel electrode set ups as opposed to a coplanar electrode that will be used in this work.

1.5 Figures

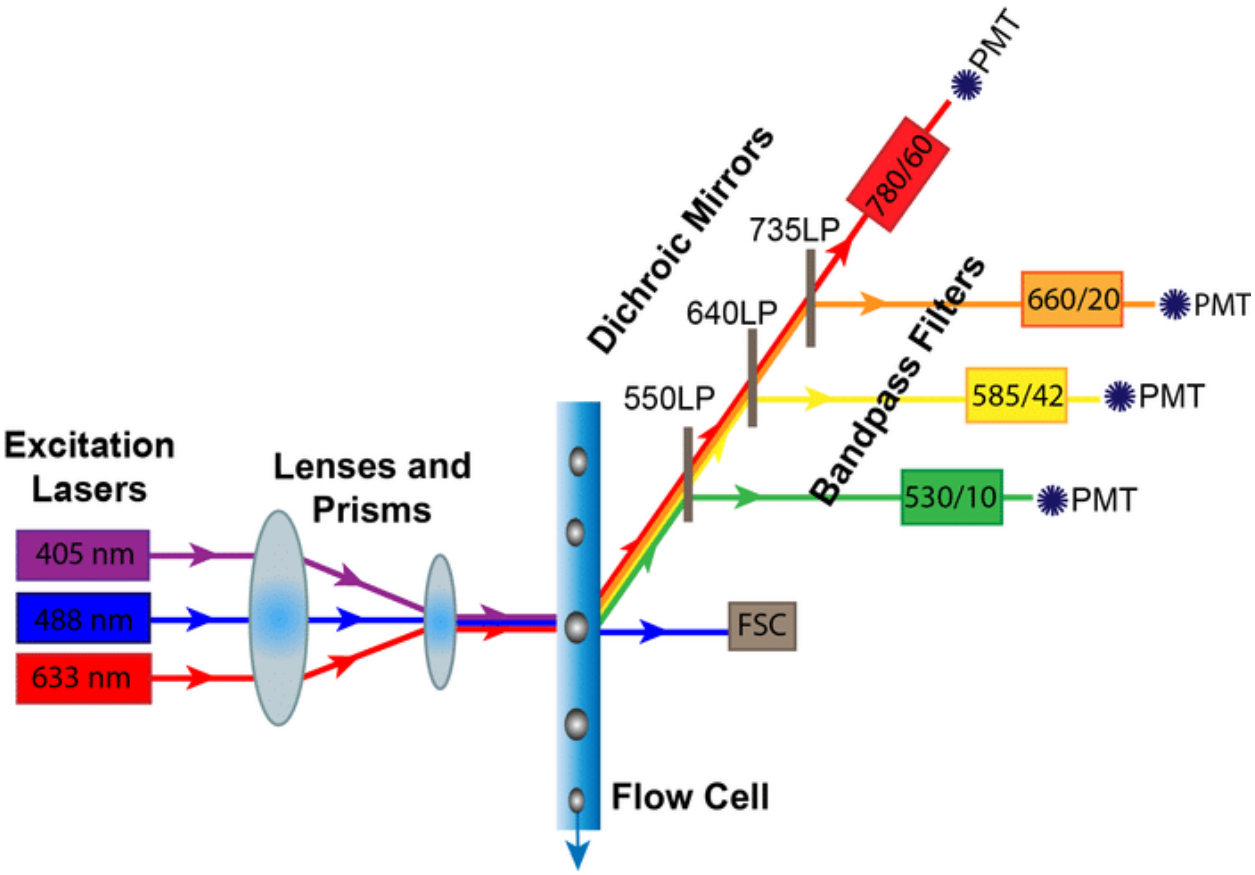

Fig. 1 Schematic showing mechanism of a flow cytometer. Cells are conjugated with fluorophores and focused into a single file line. Lasers are selected based on the fluorophore tag and used to excite the fluorophores on the cells. The intensity of light emitted by the fluorophores on a given cell can be correlated with the amount of the protein of interest on the surface of that cell. [15]

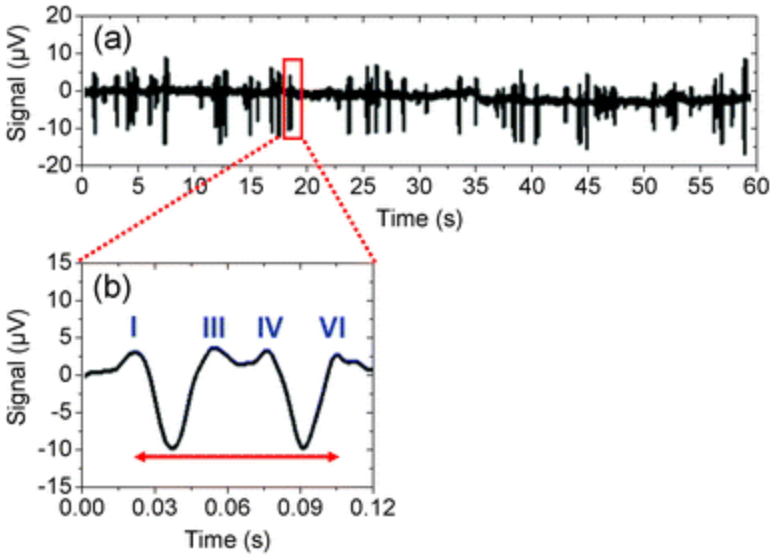

Fig. 2 Signal generated by beads flowing through a coulter counter. a) Pulse train of many beads being detected by the counter b) Zoomed in shot to show pulses caused by two individual beads. Adapted from [17]

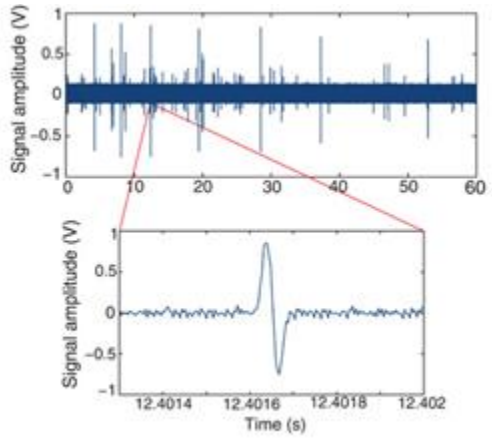

Fig. 3 Typical bipolar pulses obtained by microfluidic coulter counter as cells flow over electrodes. Top image shows multiple pulses in sequence and bottom image isolates an individual example of the bipolar pulse. Adapted from [12].

2. Simulation Design

2.1 Introduction

When running a computer simulation, it is critical to ensure that the geometry and parameters of the simulation are adjusted properly to get accurate results without taking too much computation time. The simulation was designed and run using the COMSOL Multiphysics version 5.3 software, a finite element analysis (FEA) software that allows users to combine a number of physics options and parameters in order to create a model of the device to be simulated. FEA is a technique which solves complex analytical systems by breaking them up into smaller pieces known as “finite elements”. It is particularly useful for finding boundary information and applying boundary conditions, making it well suited for the simulation of flux or gradient-based boundary conditions common in problems involving electrical fields [21].

2.2 Simulation Geometry

The simulation geometry refers to the physical structures and boundaries being simulated within the software. It is possible for COMSOL to model and simulate both 2D and 3D geometries, but for the purpose of this study a 3D simulation was used in order to ensure the highest degree of accuracy. In our simulation, the geometry of the channel was based on the counting channel of the existing chip design for a microfluidic device for the diagnosis of HIV/AIDS (Fig. 4) [28]. In order to make the geometry as flexible as possible, all aspects of the geometry were created directly in COMSOL rather than importing the geometry from CAD software. This allowed us to easily alter the geometry when needed by attaching parameters to core geometric variables such as electrode size and spacing. The main channel was modelled as a 350000 nm by 15000 nm by 15000 nm block. The length of the channel was set high in case extra space was needed for tests that would involve varying the length or spacing of the electrodes.

The electrodes being modelled were composed of a 75 nm layer of platinum mounted on a 25 nm layer of titanium. In order to model the three electrodes, three blocks were created with a height of 25 nm and set to start at the base of the channel, and three more blocks were created with a height of 75 nm that started 25 nm over the base of the channel, effectively

putting them right on top of the first layer. In order to ensure uniform spacing was maintained while allowing for changes to the electrode width and/or spacing, the electrode width and spacing were made into parameters named “electrode_w” and “electrode” respectively, both of which were defined in microns. The x-positions of the electrodes were then set so that the spacing between electrodes was equal to the “electrode” parameter, while accounting for the width parameter “electrode_w”. To do this, the first electrode was given an x-position of 50 microns, and equations were used for the second and third electrode. the second’s position was set equal to “1000*(50+electrode+electrode_w)” and the final electrode’s position was set equal to “1000*(50+2*(electrode+electrode_w))”.

The particle was modelled as either a single sphere for the initial tests. The position was made to be the center of the channel by setting both the y and z coordinates of the sphere’s center equal to the halfway point. For the x coordinate of the particle the parameter “pos” was defined. The size of the particle was defined by setting the radius of the sphere equal to a parameter called “size”.

Later tests involved modeling the particle as a multilayered sphere rather than a single homogenous one, and thus required adjustments to the particle’s geometry. This was done by adding a second concentric sphere inside of the first. A new parameter was defined as “outerthick” that would represent the thickness of the outerlayer. The larger sphere’s radius was set using the size parameter, and the inner sphere’s radius was defined as “size-outerthick”. As with the single sphere model, the center of both spheres was set with x coordinate of “pos” and y and z coordinates equal to 7500 nm.

Examples of what the final geometry looks like in the software as well as demonstrations of the flexible nature of the geometry can be seen in figures 6-8.

2.3 Simulation Physics

COMSOL Multiphysics provides an array of physics options that can be included to create a model for simulation. These are necessary to simulate the interactions of different aspects of the model and get a pertinent result. Of these physics packages, only the electrical current physics package was used in COMSOL for this model. This physics package allows us to simulate the electrical current flowing between the electrodes, which is crucial in order to simulate the coulter counter measurement, which relies on a change in the electrical impedance to count cells. While we had initially considered using a combination of the particle tracing and laminar fluid flow physics packages in order to simulate the flow of particles through the counter, this approach was ultimately abandoned in favor of simulating particle movement through a particle built in via the geometry and a parametric sweep.

The electrical current physics package was set up to include three terminals, one for each electrode, a ground, as well as the default current conservation and electric insulation. The ground was placed on the boundary below the middle electrode. Terminals were chosen to simulate the electrodes due to the ability to easily read the output voltage of a given terminal in the results, which is necessary to create the pulses we are trying to measure. The terminal corresponding to the middle electrode was set to the “voltage” terminal type which allows us to have it output a constant voltage. The voltage was set to be a parameter “Volts” which allowed it to be easily changed when testing variables. The other two terminals were set to terminal type “circuit” which gave them a default voltage of zero but still allowed voltage and current to change based on the presence of other electric fields, making it the ideal type for the two electrodes that are being directly measured to obtain the pulses.

2.4 Simulation Materials

For this study it was important to correctly assign materials and their properties to all the different parts of the system. The materials of the channel and electrodes were based upon the same chip design as the geometry [28]. The bottom of the channel was assigned the predefined PDMS material properties from COMSOL’s built in material library. Similarly, the channel walls were assigned the predefined borosilicate material properties from the COMSOL material

library. The upper layer of each electrode was assigned the platinum material properties and the lower the titanium material properties. For the bulk of the channel, a custom made "solution" material was created by starting with the built-in water from the material library and altering the electrical conductivity to 1.5 S/m based on the specifications of the solution used in the real counterpart to this design.

The particle was modeled as several possible materials depending on the test in question. For the single sphere tests, the particle was considered to be a simple polystyrene bead. As such the polystyrene properties from COMSOL's material library were used. However, since COMSOL's built in polystyrene properties did not include its electrical properties, a conductivity of $1*10^{-16}$ S/m and a relative permittivity of 2.8 [29] were added. For the double sphere tests, there were bead based simulations and cell-based simulations. Most of the bead simulations, we used polystyrene as the material of the inner sphere and either the built-in gold or a magnetite for the outer layer material. Additionally, there is also one bead based on a real bead used in experiments that has been modeled that uses a polystyrene shell around an iron core. For the magnetite, as it was not available in the COMSOL material library, a custom magnetite material was created with an electrical conductivity of 10000 S/m [30]. The iron for the iron core uses the built in iron [solid, polished] material from COMSOL's material library. For the cell based simulations, the outer shell was considered to be a plasma membrane and the inner sphere was based on the cytoplasm of a white blood cell. The values for the electrical properties were entered into a custom made cell membrane and cell cytoplasm material based on literature findings from white blood cells [31].

2.5 Computational Settings

The simulation was computed using the frequency domain study type in COMSOL, which allows us to model the current as an AC current with a chosen frequency. The frequency was set to a parameter "Freq" that is defined in kHz. The mesh was set to COMSOL's predefined extra fine setting in order to properly model the system considering the small size of the electrodes relative to the rest of the system. A parametric sweep was created in order to simulate the flow of the particles. The parametric sweep creates a set of simulations as a given

parameter, in this case the x-position parameter “pos”, is varied. A start value of 30 was chosen to start the bead a bit before the first electrode, and an end position was chosen as needed to ensure that it would end after the last electrode finished. For the single sphere tests the parametric sweep incremented “pos” by values of 0.5 until it reached the end value, but the double sphere tests increased the interval to a value of 2 in order to save computational time.

2.6 Figures

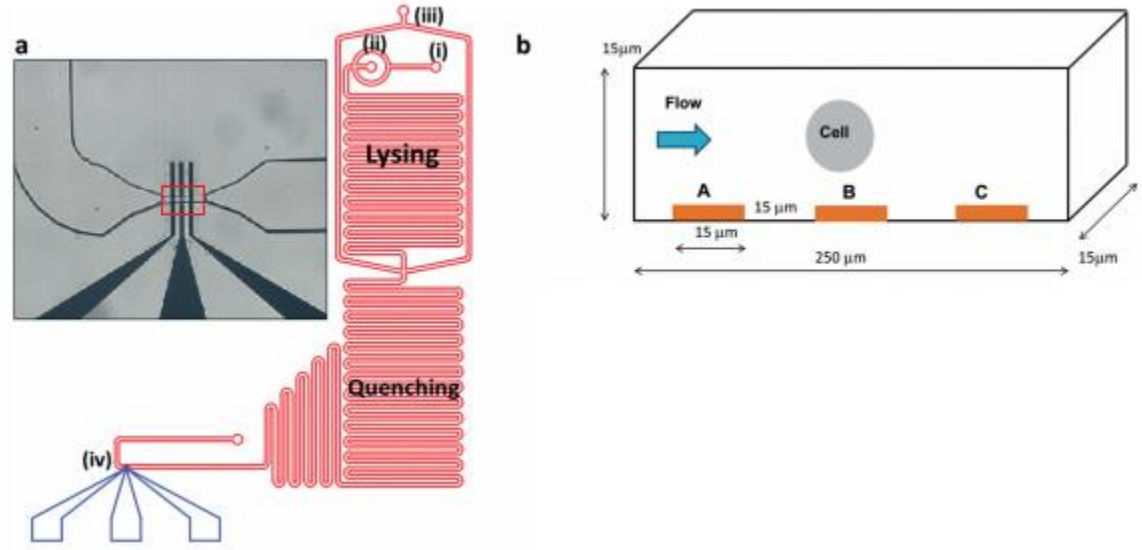

Fig. 4 a) Design of chip used as base for simulations, specific area modeled is outlined in red. b) Diagram of layout of counting channel. A, B, and C are electrodes, with voltage being input through electrode B. Adapted from [27]

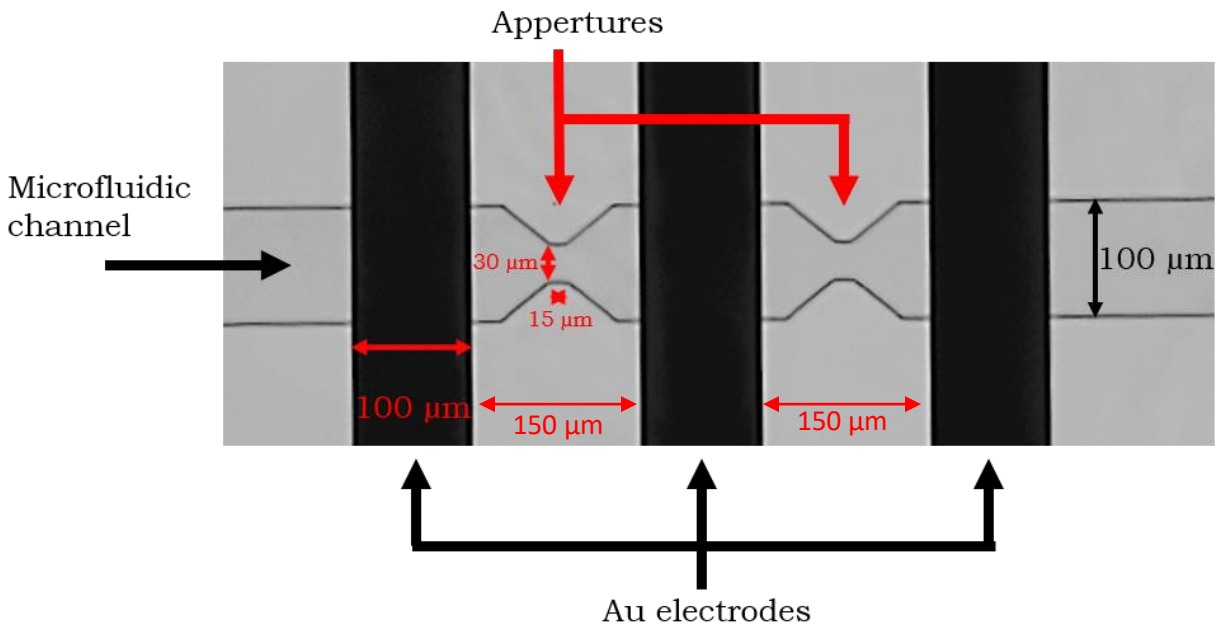

Fig. 5 Another chip design used for comparison simulations. Adapted from [28]

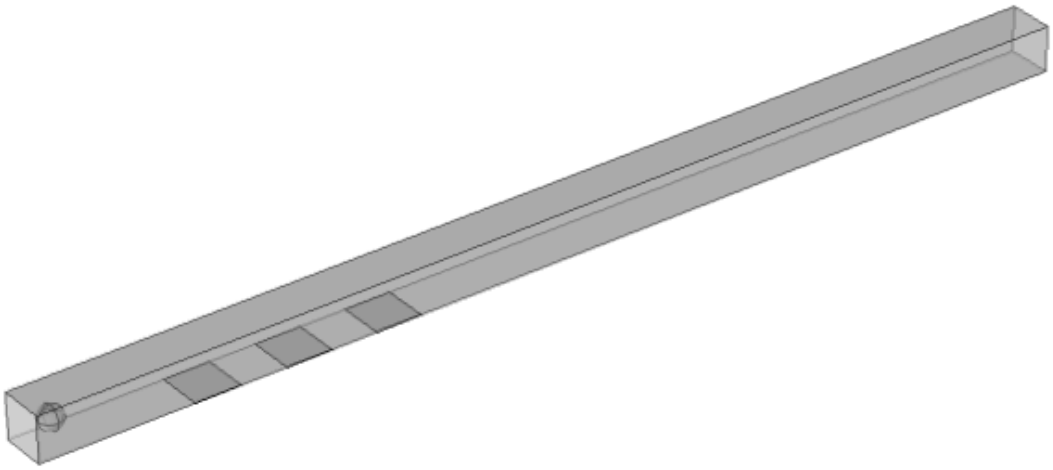

Fig. 6 Picture of standard geometry as seen in COMSOL

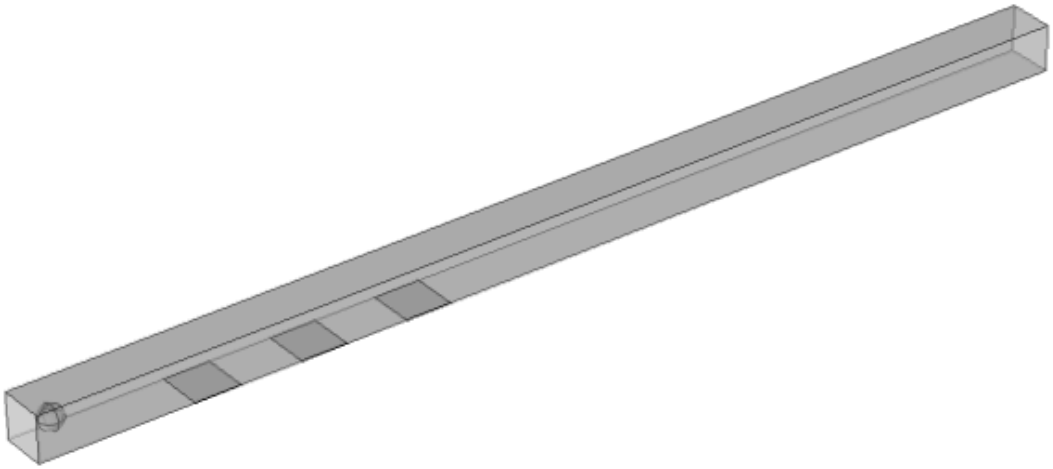

Fig. 7 Example of how Geometry in COMSOL can be modified: greater spacing between electrodes

14

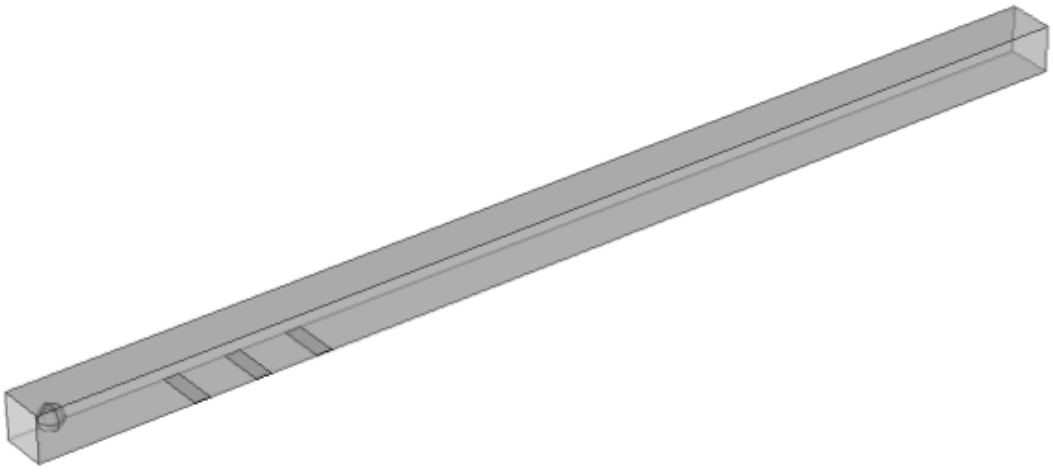

Fig. 8 Example of how COMSOL geometry can be modified: Smaller electrode width

3. Results and Discussion

3.1 Introduction

In order to test this model, several parameters were varied. The chosen variables were particle size, input voltage, input frequency, spacing between electrodes, and electrode width. These variables were chosen either because they are known to be related to coulter counter signals or because they are aspects that could feasibly be changed when optimizing chip design. This set of tests was all done using the single layer spheres simulated as being polystyrene. Additionally, double layered particles were also tested based on various bead types that might be used in testing the chip. Finally, tests were done using the double layered particle model in order to simulate different types of white blood cells that might be counted.

In order to ensure that each variable could be analyzed separately, control values were established for each of the variables. The control values are as follows: 4 micrometer radius for particle size, 5 volts for voltage, 15 micrometer electrode spacing, 15 micrometer electrode width, and 200 kilohertz for the frequency. In any test, where a specific variable of this list was not being varied, it should be assumed that it matches the control value. The notable exception is that for the white blood cell tests cell size was chosen based on the typical size of such a white blood cell.

The initial goal of this model was to be able to generate the bipolar pulse that characterizes the signal of these coulter counters as seen in Fig. 1. These were measured by taking the difference between the voltage at the first electrode and the voltage at the third electrode in order to reduce noise. This voltage was then set against the “pos” parameter which corresponds to the x-position of the center of the particle. This differs slightly from experimental results which measured voltage against time instead, however as the channel is of uniform area it can be assumed the velocity of the particles are approximately constant and thus the position of the sphere can be directly correlated to time passed at a given speed. Using the control, we were able to generate a bipolar pulse that seems to match with the general shape seen in the experimental results (Fig. 9). While the peaks are of a significantly lower amplitude than in experimental results, we believe this can be accounted for when considering

some differences in geometry with the actual chips used as well as the model not taking into account the processing the signal goes through after generation but before display, which includes amplification of the signal.

3.2 Input Voltage Tests

The first set of tests conducted was increasing the input voltage to see how this would affect the signal. Since our output signal is based on the voltage sensed by the outer electrodes as the particle interferes with the current formed from the middle electrode, we would expect a positive linear relationship between the output voltage amplitude and the input voltage. To test this, the input voltage was varied from 5 volts to 100 volts at intervals of 5 volts and then the study was computed. Results were exported from COMSOL and the highest absolute value of the second peak was determined from the signal in order to generate a graph (Fig. 10).

As expected, the relationship observed in the model was approximately linear. While not a perfect relationship, this can be attributed largely to some computational noise.

3.3 Particle Size Tests

Particle size was chosen as a tested variable because it is known that bigger particles should produce a larger signal in a coulter counter. Since the signal should be related to particle volume, we would expect that a cubic relationship might exist between the radius of the particle and the maximum signal difference obtained. To test the maximum signal difference obtained we varied the radius from 4 to 7 microns in increments of 0.5 microns. These boundaries were chosen because the diameter of the particle needs to be less than 15 microns to fit through the channel and below 4 microns the signal was not clear enough compared to any noise. Results were generated as they were with the previous test (Fig. 11).

While the resulting graph displays a clear curved relationship, it did not appear to be purely cubic in nature. To examine the relationship between volume and particle size more closely, another graph was formed by converting the particle radius to a volume by using the $4/3\ \pi\ R^3$ formula for the volume of a sphere (Fig. 12). This confirmed that the relationship between volume and size was indeed non linear as a clear, if slight, curve is still present in this graph. It is worth noting these results might be different if we had used two layers for these tests, as the

volume would then be made of a non-uniform conductivity and both layers would not be growing evenly in such a scenario.

3.4 Electric Frequency Tests

We chose frequency as the next variable to test as one of the inputs into the chip is the frequency of the AC current. To conduct this test, frequencies were chosen from 100 KHz to 2 MHz in increments of 100 kHz. These frequencies were input into the frequency domain study and then results were collected as previously (Fig. 13). Since all frequencies tested were very high, it was expected that the frequency would not show any noticeable effects on the received signal.

As expected, the results showed a fairly flat linear relationship between frequency and the change in signal. While it was not completely constant, this can likely be attributed to the computational noise and these changes can be dismissed as largely insignificant.

3.5 Electrode Spacing Tests

The spacing between the electrodes is a factor we can control to some extent during fabrication, so it was chosen as another variable for this study. In this case, all electrodes would be uniformly spaced out based on the “electrode” spacing parameter. To test this variable, the parameter was tested using values from 5 to 40 microns at 5 micron intervals. Additionally, a 3 micron data point was also collected after looking at the graph to clarify the trend. The resulting graph shows that the value does not seem to make a huge difference for the pulse amplitude, although for unknown reasons there seems to be a small increase at the 5 micron spacing data point (Fig. 14). This is likely due to computational noise, but should be noted nonetheless.

3.6 Electrode Width Tests

The electrode width is another factor that can be modified during chip fabrication, so it was also chosen for this study. All electrodes were set to have a width equal to the “electrode_w” parameter. This parameter was varied from 5 to 25 in increments of 5 microns. The resulting graph shows that increasing the electrode width will increase the produced signal to a point, but will eventually reach a peak and start going down again (Fig. 15). Further tests are likely

needed to determine whether any of the other variables such as particle size or electrode spacing could influence the best value of the electrode width.

3.7 Double Layer Tests

Most of the beads being used for the experimental chips, as well as blood cells, are composed of multiple distinct layers with different electrical properties. To investigate this, we tested double layer bead models as well as the single layer previously used. The first double layer model we tested have both layers as polystyrene, which was used as a control to ensure that the creating two layers on beads in COMSOL wasn't altering the results. Once we verified that the results were not significantly different from the single layer results, we tested the following different bead-based systems: a polystyrene core with a magnetite shell, a polystyrene core with a gold shell, and an iron core with a polystyrene shell. Finally, we also tested two cell-based models. The first was based on a lymphocyte with a 8 micron diameter, and the second was based on a granulocyte with a 12 micron diameter. A comparative bar graph shows that the main concern with the material is the conductivity of the outer layer, and more specifically whether or not it is higher or lower than the surrounding solution's conductivity (Fig. 16). This can be seen with all the particle types of the same size with lower conductivity outer shells (iron core, double layer polystyrene, and cells) producing similar signals given a similar size, and all the particle types with higher conductivity outer shells (gold shell, magnetite shell) also providing similar signals. It is worth noting that the two high conductivity shell types produced the greatest amplitude, suggesting they may be the best choice for actual experiments. Another interesting note is that the two higher conductivity types produced inverted signals compared to the previous types, with the first peak being positive and the second being negative (Fig. 17).

3.8 Experimental Data

In order to directly compare the shape of the simulation to experimental results, the simulated curve from the lymphocyte test data was transformed to match the general amplitude and width of an experimental curve taken from a lymphocyte going through an experimental chip (Fig. 18). This shows that the general shape of each pulse looks generally correct. Similar comparisons were made for granulocyte data, and again the results matched up

nicely (Fig. 19). While the multipliers were different for the granulocyte and lymphocyte, this can be explained by real cells coming in a range of sizes, so it could be that a small granulocyte and a large lymphocyte were measured in the experimental pulse, leading to the sizes of the cells measured not exactly matching up with the simulated sizes. The slight difference in the time multiplier might be explained by slight variations of speed in the chip due to some imprecision of the technology.

Additionally, experimental data for 7-micron diameter polystyrene beads, and two sizes of magnetic beads have been included here (Fig. 20-22). The shapes for these differ from the current simulated results due to differences in chip design, however they show similar trends for how changing variables changes the final amplitude of the pulses as the simulated data.

3.9 Figures

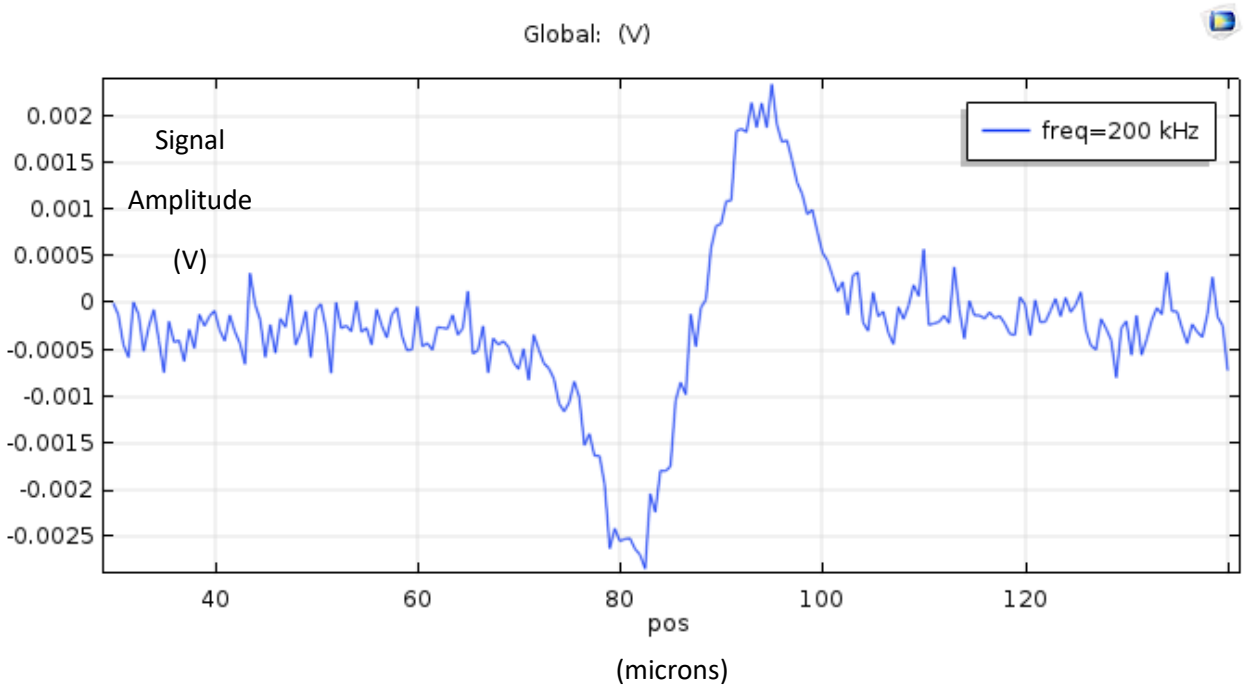

Fig. 9 Graph of voltage difference against x position for control test. Shows bipolar pulse similar to what can be seen in Fig. 3

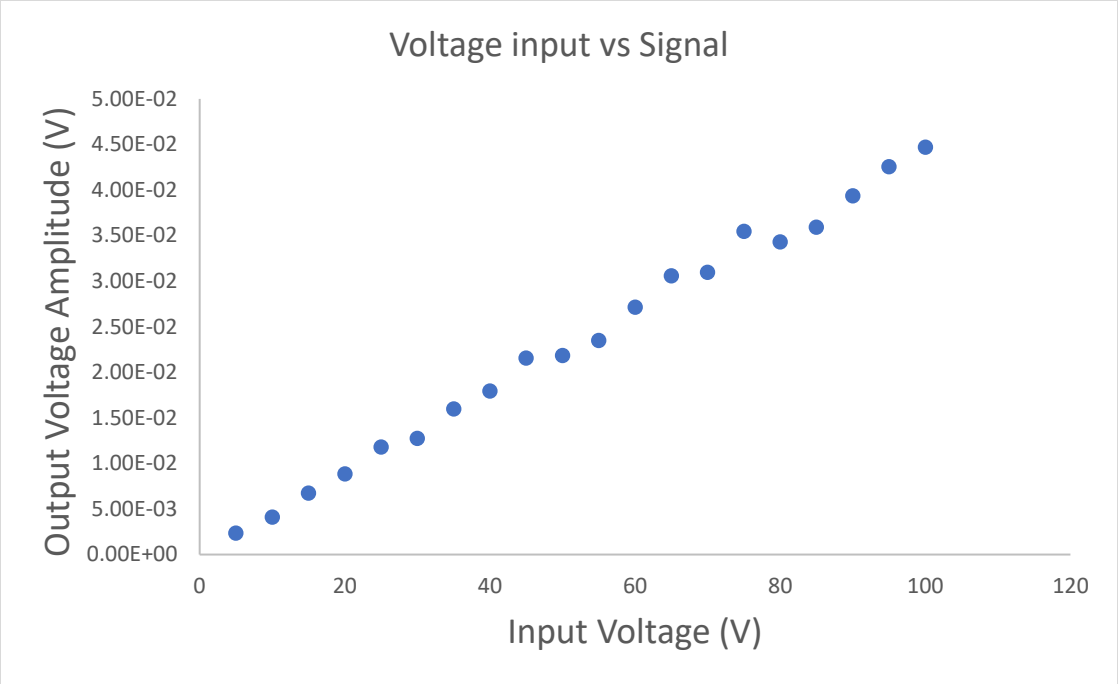

Fig. 10 Input voltage at middle electrode vs output voltage amplitude for second of the bipolar peaks

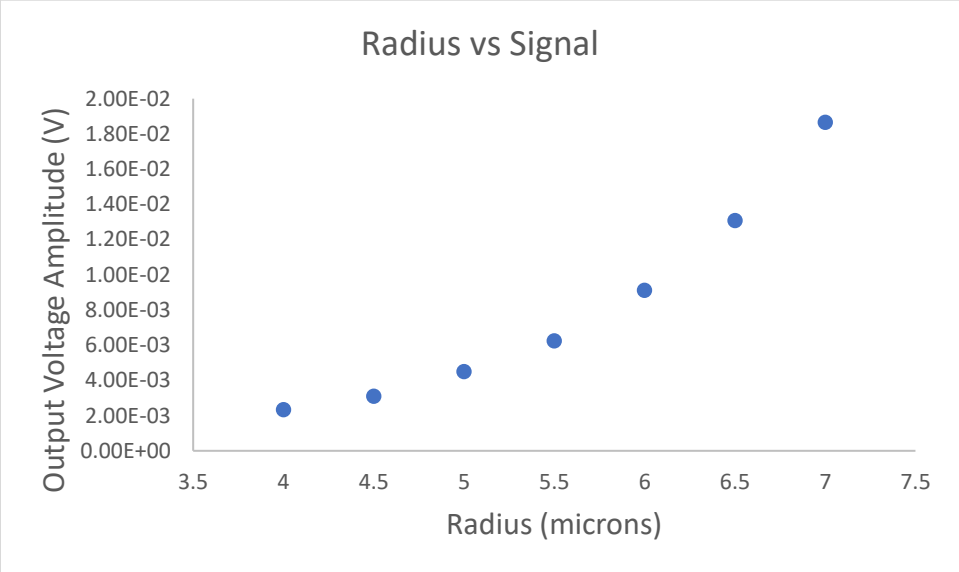

Fig. 11 Particle radius vs output voltage amplitude for second of the bipolar peaks

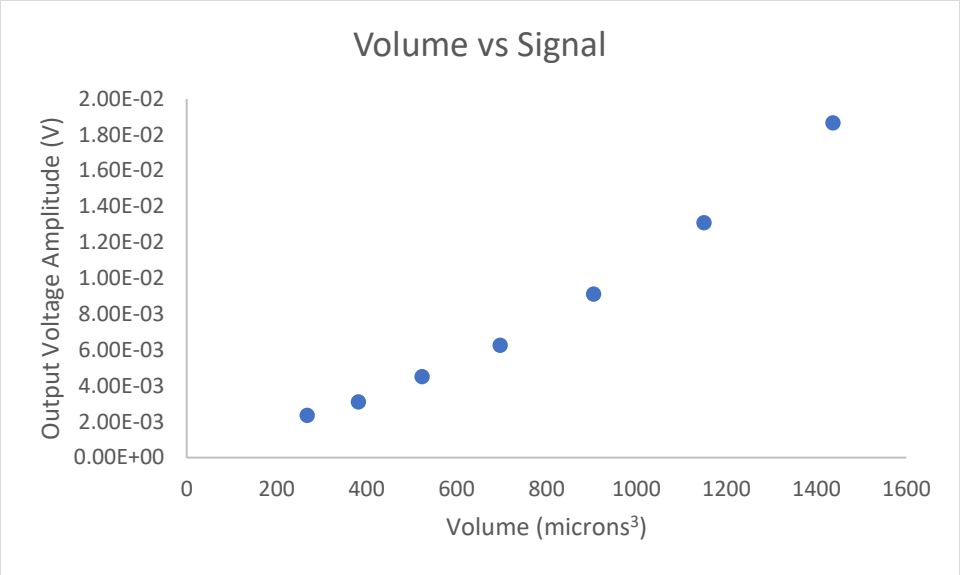

Fig. 12 Particle volume vs output voltage amplitude for second of the bipolar peaks. Volume numbers obtained by converting from radius using volume of a sphere

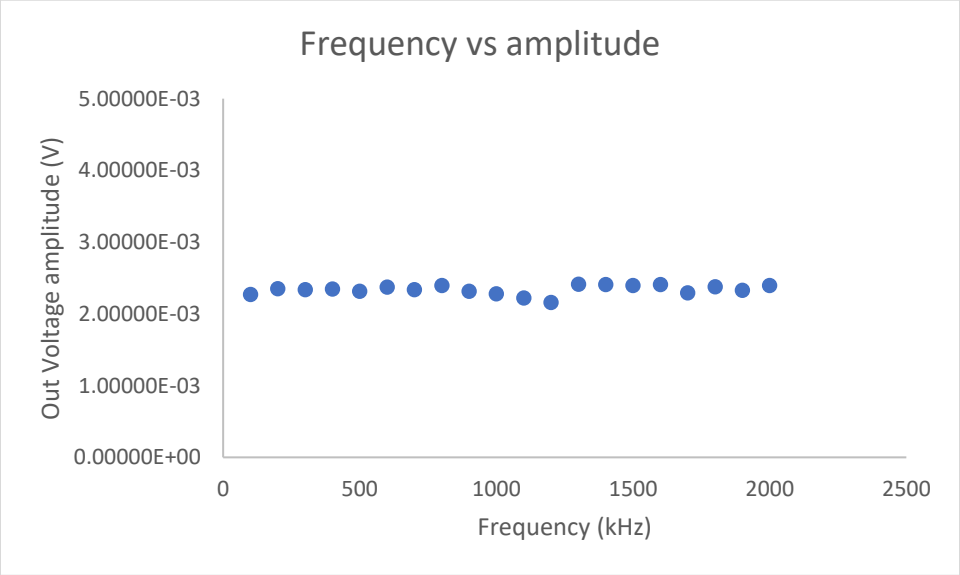

Fig. 13 AC current frequency vs output voltage amplitude for second of the bipolar peaks

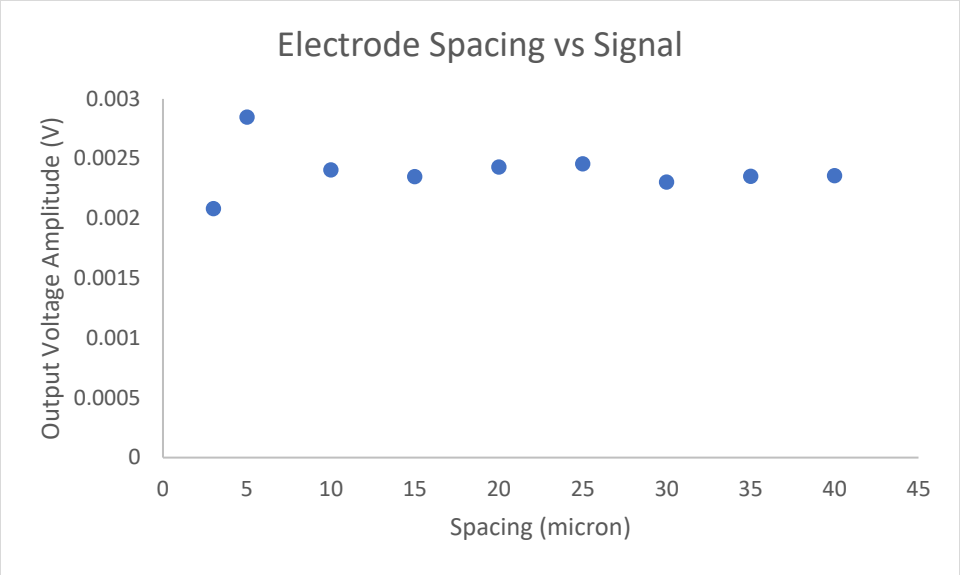

Fig. 14 Spacing between electrodes vs output voltage amplitude for second of the bipolar peaks

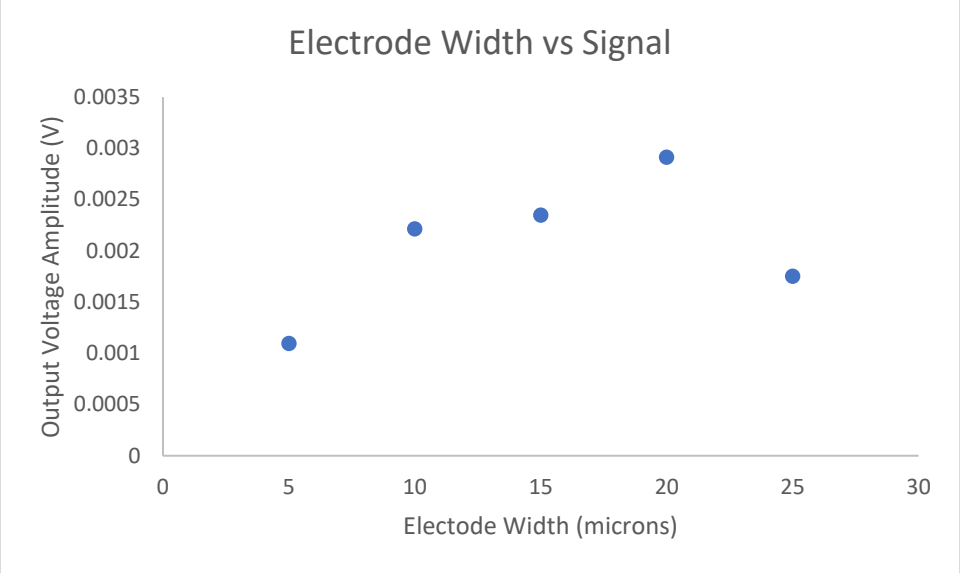

Fig. 15 Electrode width vs output voltage amplitude for second of the bipolar peaks

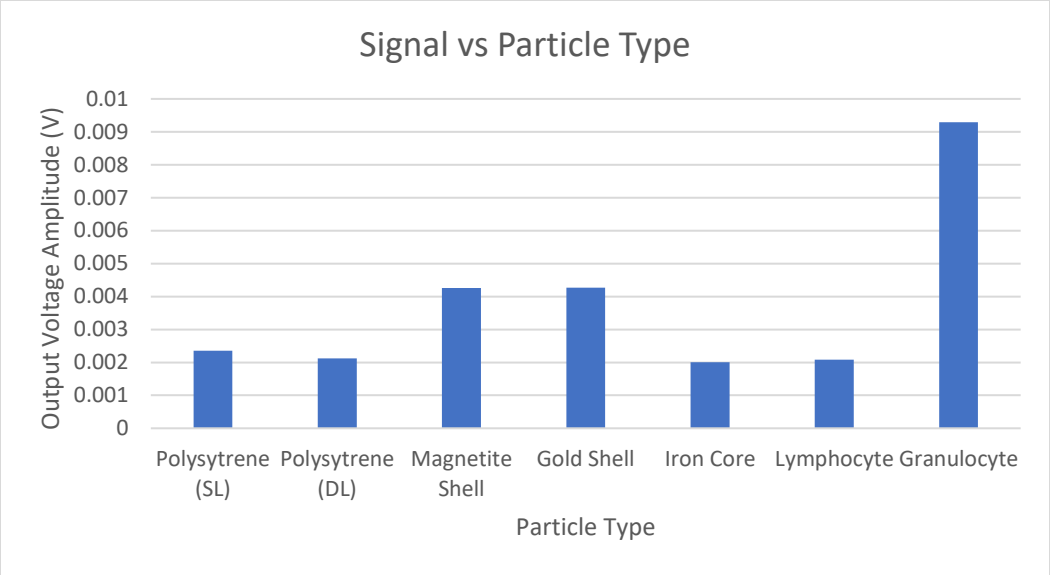

Fig. 16 Particle types vs output voltage amplitude for second of the bipolar peaks. Types were: polystyrene single layer (Polystyrene (SL)), polystyrene double layer (Polystyrene (DL)), polystyrene core with magnetite shell (Magnetite Shell), polystyrene core with gold shell (Gold Shell), iron core with polystyrene shell (Iron Core), Lymphocyte cell (Lymphocyte), and Granulocyte cell (Granulocyte)

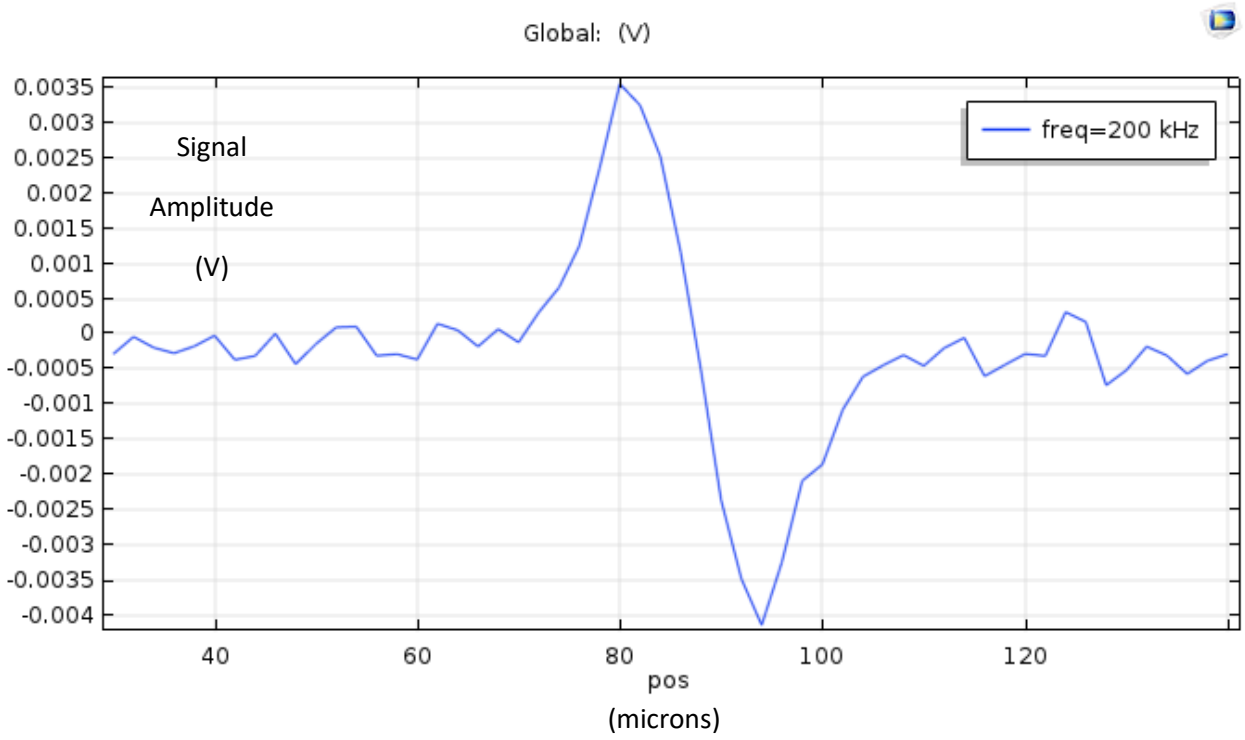

Fig. 17 Graph of voltage difference against x position for Magnetite Shell test. Pulse is inverted compared to tests where outer layer is composed of low conductivity material such as the pulse in Fig. 6

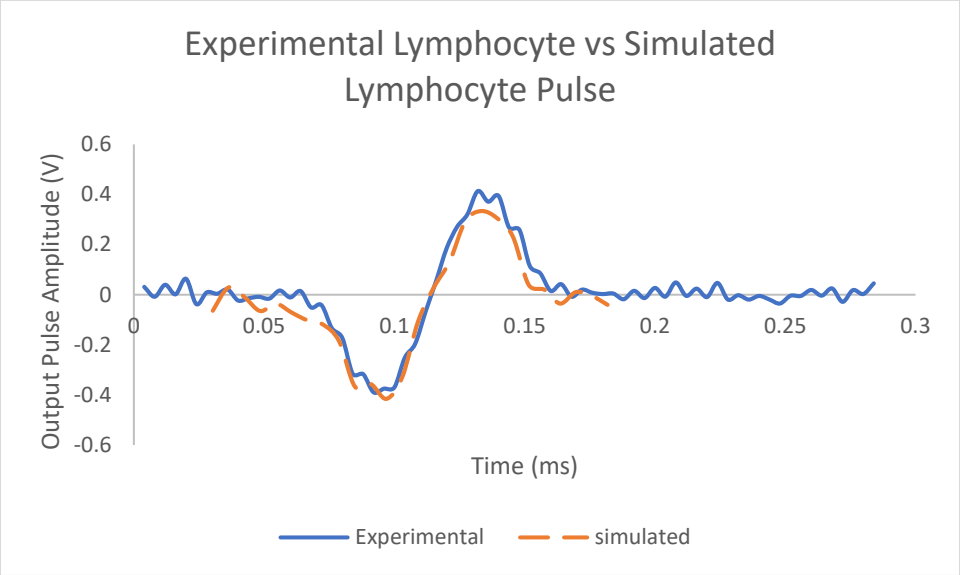

Fig. 18 A comparison of curve shape for experimental lymphocyte results vs simulated lymphocyte results. Simulated results were transformed by multiplying amplitude by 160. Additionally, the x-position parameter in the simulated results was converted to time by the following formula: t=(pos-50)/330 so that it could best match up with the experimental curve

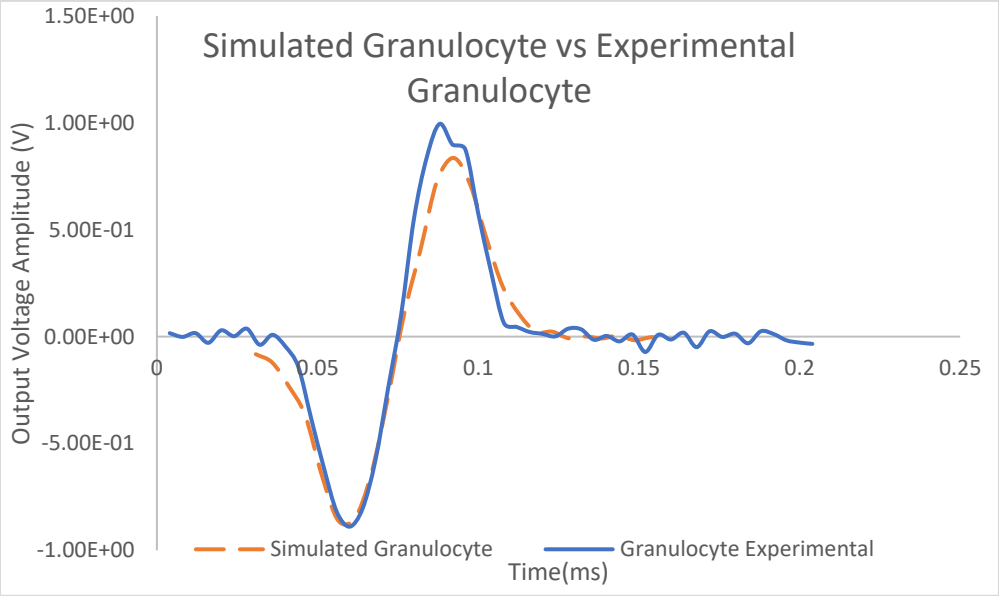

Fig. 19 A comparison of curve shape for experimental lymphocyte results vs simulated lymphocyte results. Simulated results were transformed by multiplying amplitude by 90.

Additionally, the x-position parameter in the simulated results was converted to time by the following formula: t=(pos-58)/390 so that it could best match up with the experimental curve.

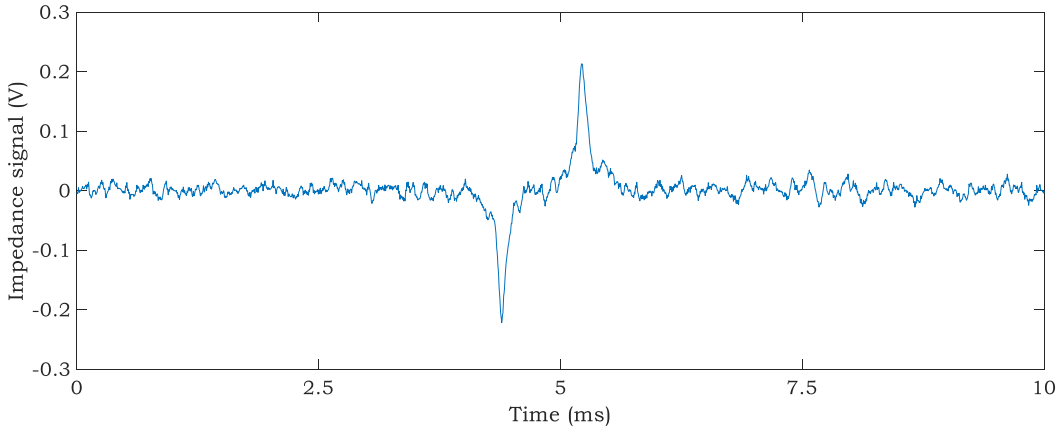

Fig. 20 Signal Produced in experimental tests with 7 micron diameter polystyrene beads

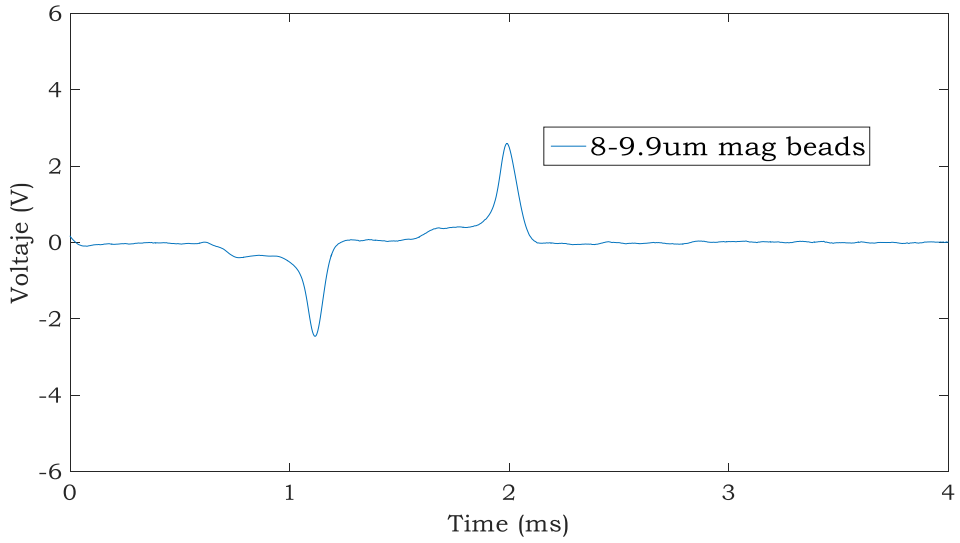

Fig. 21 Signal produced in experimental tests with 8-9.9 micron diameter magnetic beads

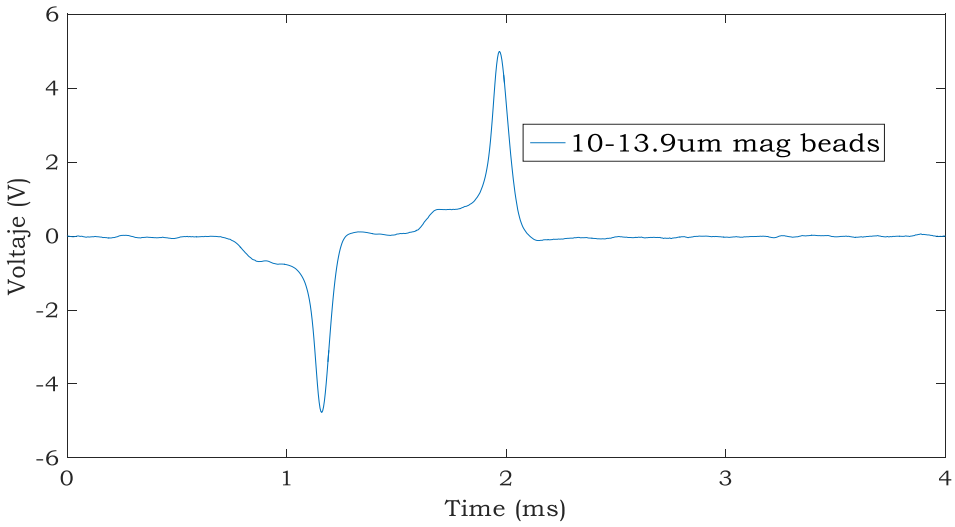

Fig. 22 Signal Produced in experimental tests with 10-13.9 diameter micron magnetic beads

4. Conclusions and Future Work

We have created a simulation that can model a microfluidic coulter counter that uses three coplanar electrodes in order to produce a bipolar pulse. We have demonstrated the model's ability to assess the effects of multiple variables on the amplitude of the signal that the coulter counter provides.

Based on the results we can see that increasing particle size appears to be the most efficient method for increasing the signal amplitude of the coulter counter. However, we must consider that due to the channel height, making a particle too large will stop it from being able to flow through the channel. As such, one area of future work to look into would be to see how channel height affects the signal of the coulter counter. Additionally, since both cells and many bead types have multiple layers, it would be worth looking into how varying the thickness of those layers independently changes the produced signal for multiple particle types.

Additional future work could also include varying the shape of the channel and/or particles to see how this affects the output. It may also be worth looking into different electrode arrangements in order to see how the produced signal compares and see if their might be a more efficient arrangement. Another important area of future work is adapting the design of the channel in order to be more in line with what is being used in more current chip iterations.

References

1. D. F. Gaieski, J. M. Edwards, M. J. Kallan, and B. G. Carr, "Benchmarking the Incidence and Mortality of Severe Sepsis in the United States*," *Critical Care Medicine*, vol. 41, no. 5, pp. 1167–1174, 2013.
2. N. K. Adhikari, R. A. Fowler, S. Bhagwanjee, and G. D. Rubenfeld, "Critical care and the global burden of critical illness in adults," *The Lancet*, vol. 376, no. 9749, pp. 1339–1346, 2010.
3. R. Daniels, "Surviving the first hours in sepsis: getting the basics right (an intensivists perspective)," *Journal of Antimicrobial Chemotherapy*, vol. 66, no. Supplement 2, pp. ii11–ii23, Nov. 2011.
4. V. N. Umlauf, S. Dreschers, and T. W. Orlikowsky, "Flow Cytometry in the Detection of Neonatal Sepsis," *International Journal of Pediatrics*, vol. 2013, pp. 1–6, 2013.
5. S. Zanotti-Cavazzoni, "Duration of hypotension before initiation of effective antimicrobial therapy is the critical determinant of survival in human septic shock," *Yearbook of Critical Care Medicine*, vol. 2007, pp. 187–188, 2007.
6. P. Yager, T. Edwards, E. Fu, K. Helton, K. Nelson, M. R. Tam, and B. H. Weigl, "Microfluidic diagnostic technologies for global public health," *Nature*, vol. 442, no. 7101, pp. 412–418, 2006.
7. C. D. Chin, T. Laksanasopin, Y. K. Cheung, D. Steinmiller, V. Linder, H. Parsa, J. Wang, H. Moore, R. Rouse, G. Umviligihozo, E. Karita, L. Mwambarangwe, S. L. Braunstein, J. V. D. Wijgert, R. Sahabo, J. E. Justman, W. El-Sadr, and S. K. Sia, "Microfluidics-based diagnostics of infectious diseases in the developing world," *Nature Medicine*, vol. 17, no. 8, pp. 1015–1019, 2011.
8. U. Hassan, T. Ghonge, B. R. Jr., M. Patel, M. Rappleye, I. Taneja, A. Tanna, R. Healey, N. Manusry, Z. Price, T. Jensen, J. Berger, A. Hasnain, E. Flaugher, S. Liu, B. Davis, J. Kumar, K. White, and R. Bashir, "A point-of-care microfluidic biochip for quantification of CD64 expression from whole blood for sepsis stratification," *Nature Communications*, vol. 8, p. 15949, Mar. 2017.

9. V. Gubala, L. F. Harris, A. J. Ricco, M. X. Tan, and D. E. Williams, “Point of Care Diagnostics: Status and Future,” *Analytical Chemistry*, vol. 84, no. 2, pp. 487–515, 2011.
10. R. Fang, O. Vermesh, A. Srivastava, B. K. H. Yen, L. Qin, H. Ahmad, G. A. Kwong, C.-C. Liu, J. Gould, L. Hood, and J. R. Heath, “Integrated Blood Barcode Chips,” *Nature Biotechnology*, Nov. 2008.
11. C. V. Berkel, J. D. Gwyer, S. Deane, N. Green, J. Holloway, V. Hollis, and H. Morgan, “Integrated systems for rapid point of care (PoC) blood cell analysis,” *Lab on a Chip*, vol. 11, no. 7, p. 1249, 2011.
12. N. N. Watkins, U. Hassan, G. Damhorst, H. Ni, A. Vaid, W. Rodriguez, and R. Bashir, “Microfluidic CD4 and CD8 T Lymphocyte Counters for Point-of-Care HIV Diagnostics Using Whole Blood,” *Science Translational Medicine*, vol. 5, no. 214, Apr. 2013.
13. F. S. Apple, F. P. Anderson, P. Collinson, R. L. Jesse, M. C. Kontos, A. Levitt, E. A. Miller, and M. A. M. Murakami, “ Clinical Evaluation of the First Medical Whole Blood, Point-of-Care Testing Device for Detection of Myocardial Infarction,” *Clinical Chemisty*, vol. 26, no. 10, Oct. 2000.
14. M. Brown and C. Wittwer, “Flow Cytometry: Principles and Clinical Applications in Hematology,” *Clinical Chemisty*, vol. 46, no. 8, 2000.
15. “Demystifying the Flow Cytometry Optics System: A Peek Under the Hood,” *Bitesize Bio*, 22-Nov-2016. [Online]. Available: https://bitesizebio.com/31638/flow-cytometry-optics-system/. [Accessed: 28-Mar-2018].
16. W. H. Coulter, “Coulter, WH. Means For Counting Particles Suspended In A Fluid,” 20-Oct-1953.
17. J. Zhe, A. Jagtiani, P. Dutta, J. Hu, and J. Carletta, “A micromachined high throughput Coulter counter for bioparticle detection and counting,” *Journal of Micromechanics and Microengineering*, vol. 17, no. 2, pp. 304–313, Nov. 2007.
18. M. Helou, M. Reisbeck, S. F. Tedde, L. Richter, L. Bär, J. J. Bosch, R. H. Stauber, E. Quandt, and O. Hayden, “Time-of-flight magnetic flow cytometry in whole blood with integrated sample preparation,” *Lab on a Chip*, vol. 13, no. 6, p. 1035, 2013.

19. J. Guo, H. Li, Y. Chen, and Y. Kang, “A Microfluidic Impedance Cytometer on Printed Circuit Board for Low Cost Diagnosis,” *IEEE Sensors Journal*, vol. 14, no. 7, pp. 2112–2117, 2014.
20. D. Holmes, D. Pettigrew, C. H. Reccius, J. D. Gwyer, C. V. Berkel, J. Holloway, D. E. Davies, and H. Morgan, “Leukocyte analysis and differentiation using high speed microfluidic single cell impedance cytometry,” *Lab on a Chip*, vol. 9, no. 20, p. 2881, 2009.
21. D. Erickson, “Towards numerical prototyping of labs-on-chip: modeling for integrated microfluidic devices,” *Microfluidics and Nanofluidics*, vol. 1, no. 4, pp. 301–318, 2005.
22. A. Wolff, I. R. Perch-Nielsen, U. D. Larsen, P. Friis, G. Goranovic, C. R. Poulsen, J. P. Kutter, and P. Telleman, “Integrating advanced functionality in a microfabricated high-throughput fluorescent-activated cell sorter,” *Lab on a Chip*, vol. 3, no. 1, p. 22, 2003.
23. A. Ajdari, “Electro-Osmosis on Inhomogeneously Charged Surfaces,” *Physical Review Letters*, vol. 75, no. 4, pp. 755–758, 1995.
24. C. Chen, S. Zappe, O. Sahin, X. Zhang, M. Fish, M. Scott, and O. Solgaard, “Design and operation of a microfluidic sorter for Drosophila embryos,” *Sensors and Actuators B: Chemical*, vol. 102, no. 1, pp. 59–66, 2004.
25. Y. Wu, M. Almasri, and J. D. Benson, “MEMS Coulter counter for dynamic impedance measurement of cells,” *2011 IEEE SENSORS Proceedings*, 2011.
26. Z. Mei, Z. Liu, and Z. Zhou, “A compact and low cost microfluidic cell impedance detection system,” *AIMS Biophysics*, vol. 3, no. 4, pp. 596–608, 2016.
27. J. Guo, T. S. Pui, A. R. A. Rahman, and Y. Kang, “3D numerical simulation of a Coulter counter array with analysis of electrokinetic forces,” *Electrophoresis*, vol. 34, no. 3, pp. 417–424, 2012.
28. U. Hassan and R. Bashir, “Coincidence detection of heterogeneous cell populations from whole blood with coplanar electrodes in a microfluidic impedance cytometer,” *Lab Chip*, vol. 14, no. 22, pp. 4370–4381, Jan. 2014.
29. “Material Properties of Polystyrene and Poly(methyl methacrylate) (PMMA) Microspheres,” *Bangs Laboratories, Inc.*[Online]. Available:

https://www.bangslabs.com/sites/default/files/imce/docs/TSD 0021 Material Properties Web.pdf.

30. L. Blaney, “Magnetite (Fe3O4): Properties, Synthesis, and Applications,” *Leheigh Review*, vol. 15, 2007.
31. Y. Polevaya, I. Ermolina, M. Schlesinger, B.-Z. Ginzburg, and Y. Feldman, “Time domain dielectric spectroscopy study of human cells,” *Biochimica et Biophysica Acta (BBA) - Biomembranes*, vol. 1419, no. 2, pp. 257–271, 1999.